Massive MIMO Channel Measurements and Simulations at 3.7 GHz in Outdoor Environment

Nada Bel-Haj-Maati, Nadine Malhouroux, Patrice Pajusco, Michel Ney

Massive MIMO Channel Measurements and Simulations at 3.7 GHz in Outdoor Environment

Nada Bel-haj-maati, Nadine Malhouroux
Wireless Engineering and Propagation department
Orange Labs
Belfort, France
nada.belhajmaati@orange.com
nadine.malhouroux@orange.com

Patrice Pajusco, Michel Ney
Microwave department, Lab-STICC
IMT Atlantique
Brest, France
patrice.pajusco@imt-atlantique.fr
michel.ney@imt-atlantique.fr

***Abstract*—Massive multiple-input multiple-output (MIMO) is considered as one of the building blocks of 5G. This technology offers higher capacity, faster speed and improved spectral and energy efficiency. In this paper, we investigate massive MIMO propagation channel performances in real propagation environment. Therefore, channel measurements were carried out at 3.7 GHz using a uniform planar array (UPA) with 64 elements as a receiver and a patch array made of 8 elements PIFA as a transmitter. Both line-of-sight (LoS) and non-line-of-sight (NLoS) conditions were investigated in this campaign. Additionally, simulations using Orange ray-based 3D propagation model termed as Starlight were conducted. The objective is to characterize both measured and simulated Massive MIMO channels and optimize this propagation model to ensure agreement between simulations and measurements.**

Keywords—5G, Massive MIMO, Channel Measurement, Spatio-temporal characterization, Outdoor Microcell, Simulation, Ray-tracing, Direction of Arrival

I. INTRODUCTION

The ever increasing demand for data rates and latency reduction has lead researchers and wireless engineers to develop a new generation of wireless communication, called 5G. 5G technology will allow data rates up to 10x faster than 4G, higher capacity and lower latency. 5G deployment will be based on existing 4G base stations with the integration of intelligent massive MIMO antennas that enable beamforming, and the use of two different frequency bands (3.4 – 3.8 GHz) and (24– 27 GHz). Current 4G base stations that handle all cellular traffic can use 4 antennas to transmit and 4 antennas to receive signals. However, 5G base stations can support about a hundred ports, which means that a base station could send and receive signals from many more users at once. Therefore, network capacity can be increased by a factor of 22 or greater [1].

To characterize the massive MIMO propagation channel and evaluate the system's capacity and spatio-temporal characteristics, it is important to develop an accurate channel model based on real measurements. In this paper, wideband measurements and simulations for massive MIMO system (8×64) were performed at 3.7 GHz, which is one of 5G frequencies, in an outdoor micro-cellular environment in both LOS and NLOS conditions.

This paper is organized as follows. In Section II, the measurement setup is presented. Then in Section III, the outdoor measurement campaign is described. Next, in Section IV, we present the ray-tracing tool used for simulations. In Section V and VI a description of spatio-temporal characteristics is provided, as well as measurement and simulation results are presented. Finally, Section VII concludes this paper and draws some perspectives for future studies.

II. MEASUREMENT SYSTEM DESCRIPTION

This section describes the measurement equipment and presents the setup parameters.

A. Measurement setup

The measurement was carried out using a channel sounder developed under a research contract with IMT Atlantique. It is based on real-time SDR platform and Matlab™ for post-processing. The transmitter (TX) was composed of an arbitrary waveform generator and a patch antenna array with 8 elements PIFA (Planar Inverted-F Antenna) depicted in Fig. 2. The receiving antenna (RX) "Scan 64" [2] depicted in Fig. 3 is a dual-polarized Uniform Planar Array (UPA), with 64 switched slot radiating elements (32 for horizontal polarization and 32 for vertical polarization), with a uniform spacing of $\lambda/2$. The antenna switching of TX and RX array is performed by the FPGA in the receiver. The frequency synchronization between the transmitter and the receiver is achieved with a coaxial cable (10 MHz reference).

The measurement setup is detailed in Fig. 1.

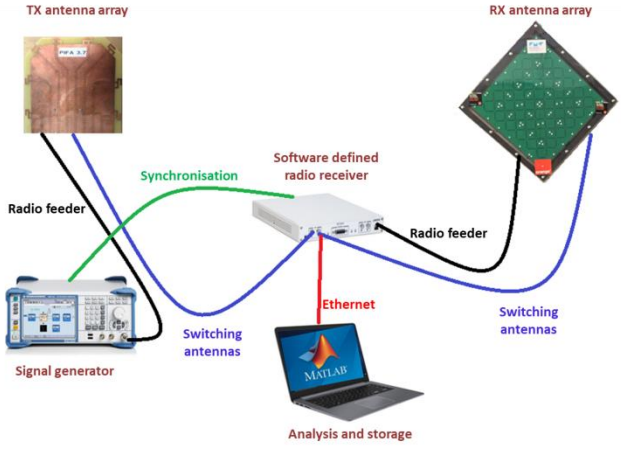

Fig. 1. Equipment setup

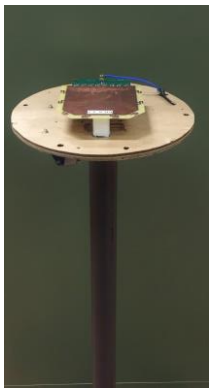

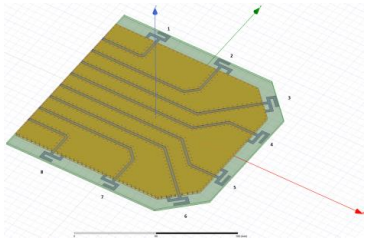

Fig. 2. The patch antenna array with 8 PIFA elements transmitter

Fig. 3. UPA 64-elements receiver

B. *Measurement parameters*

The measurements were conducted at a carrier frequency of 3.7 GHz, using the IMT Atlantique's real-time MIMO wideband channel sounder. The transmitted signal is 300-length wideband sequences with a 100-MHz channel bandwidth. Thus, the length of the measured impulse response (IR) is 3 µs. The measurement settings are presented in Table I.

TABLE I. MEASUREMENT SETTING

Carrier Frequency [GHz]	3.7
Bandwidth [MHz]	100
Length of transmitted signal [µs]	3
Transmit Power [dBm]	30
Number of transmit antenna	8
Number of receive antenna	64
Type of TX antenna array	UPA
Type of RX antenna array	PIFA

III. MEASUREMENT CAMPAIGN

The measurements campaign was performed on the Techn'hom campus of Belfort, where the Orange Labs premises are located. An overview of the measurement environment is represented in Fig. 4.

The RX antenna was mounted on the stairs at 6.5 m above ground level for all TX positions. TX antenna was placed at different positions in LoS and NLoS conditions. The distances between the RX and the 11 TX positions ranged from 9 to 54 m. Three distinctive transmission points were considered according to RX's main beam orientation: blue towards south, pink towards east and green towards north. Fig. 4 shows a picture of the RX antenna and the TX positions with their associated antenna beamwidth orientation.

Fig. 4. Overview of the measurement area

Fig. 5. Measurement environment and RX antenna position

IV. SIMULATIONS

A. *Ray-tracing tool*

To analyse the measurement results and obtain all details of multipath propagation, a software simulator was used. For our studies, we used "Starlight" [3] a 3D channel model based on ray-tracing which has been developed by Orange Labs.

From an accurate description of the propagation scene, positions of TX and RX antenna and the maximum number of considered propagation phenomena (N_{ref} reflection, N_{trans} transmission, and N_{diff} diffraction), Starlight provides a list of identified rays between the transmit and the receiving point. Each ray is characterized by a propagation delay, amplitude, DoD and DoA. Its algorithm is based on geometrical optics (GO) and its extension to the uniform theory of diffraction (UTD). Starlight operates on a 3D model of the propagation environment described by numerous surfaces which are characterized by the thickness and dielectric parameters (relative permittivity ε_r and conductivity σ) of their composing materials. Table II summarizes the materials used in our simulations, their thickness and complex permittivity ε values [4]:

$$\varepsilon = \varepsilon_r - j60\sigma\lambda \quad (1)$$

where λ is the wavelength in free space.

TABLE II. MATERIAL PROPRIETIES USED FOR SIMULATIONS (FOR FREQUENCY RANGE 1-100 GHZ)

Material	Complex permittivity	Thickness (cm)
Concrete	$\mathbf{5.31 - j0.57}$	10
Ground	$\mathbf{14.73 - j1.61}$	10

Fig. 6 shows an example of the 3D outdoor scene with different ray paths found by Starlight between the TX and RX.

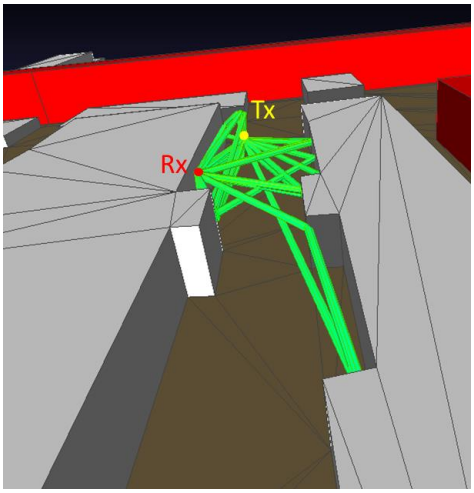

Fig. 6. An example of the 3D outdoor scene with different ray paths found between TX and RX

B. Parametrization

Ray-tracing computation time increases rapidly with the number of reflection and diffraction phenomena. That is why we choose to limit the maximum number of considered propagation phenomena in our simulations to have only useful rays. For this purpose, we investigated the evolution of total received power as a function of the number and type of phenomena taken into account. As the measurements are conducted in the same street, we choose to set the number of diffraction to $N_{diff} = 1$ and to compute the power of the rays for a mix of N_{ref} reflexions and N_{diff} diffractions.

Fig. 7 represents the evolution of the total received power of the rays versus the propagation phenomena for 2 different transmitter positions in LoS and NLoS conditions. One can observe that the power of determined rays increases significantly when incrementing N_{ref}. For TX positions in LoS, rays with 1 diffraction and more than 3 reflections do not have any significant contribution to power. After measurement analysis, in this configuration, rays with 1 diffraction and 4 reflections are sufficient.

From the above observations, a maximum number of 1 diffraction and 4 reflections are allowed for each ray for both LoS and NLoS conditions.

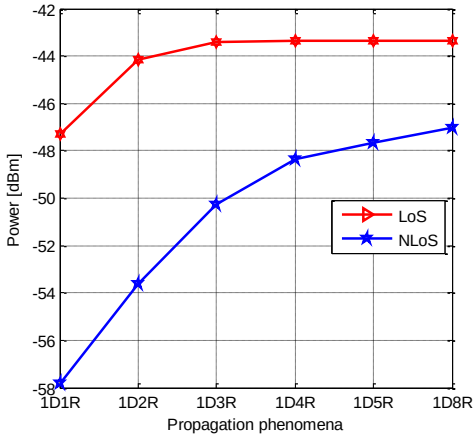

Fig. 7. Evolution of power versus type of propagation phenomena (D = diffraction, R = Reflexion)

V. PROPAGATION CHANNEL CHARACTERIZATION

To allow a fair comparison between measurements (limited bandwidth) and simulations (discrete paths), the influence of TX and RX antennas and 8T×64R massive MIMO configuration and limited bandwidth must be accounted for in our simulations. To do so, simulated transfer functions (TFs) are computed from a set of rays generated with Starlight by applying radiation patterns of "Scan 64" antenna and 8-ports PIFA. Different channel characteristics were then extracted.

A. Power delay profile and Delay spread

The power delay profile (PDP) of the different massive MIMO configuration links are computed from measurements and simulated data. It gives the distribution of signal power received over a multipath channel as a function of propagation delays. The PDP is computed as the average power, associated with each delay, between the N_{SISO} CIRs of all single input single output (SISO) links of the corresponding massive MIMO configuration:

$$PDP(\tau) = \frac{1}{N_{SISO}} \sum_{n=1}^{N_{SISO}} |h_n(\tau)|^2 \qquad (2)$$

The delay spread (DS) τ_{DS} is a parameter to characterize the multipath richness of a propagation channel. It is the relative time difference between the first signal component arriving at the receiver to the last one whose power level is above a threshold. DS is computed from PDP as shown in (3):

$$\tau_{DS} = \sqrt{\frac{\int_\tau (\tau - \tau_{mean})^2 \mathrm{PDP}(\tau)\, d\tau}{\int_\tau \mathrm{PDP}(\tau)\, d\tau}} \qquad (3)$$

$\tau_{mean} = \frac{\int_p \tau\, \mathrm{PDP}(\tau)\, d\tau}{\int_p \mathrm{PDP}(\tau)\, d\tau}$ is the mean delay, the normalized first-order moment of the PDP. In micro-cellular configuration, the delay spread is usually smaller and rarely exceeds a few hundred nanoseconds. Seidel and Rappaport [5] reported delay spreads in four European cities of less than 8 µs in macro-cellular channels, less than 2 µs in micro-cellular channels, and between 50 and 300 ns in pico-cellular channels.

B. *Directions of Arrival*

The knowledge of the direction of arrival (DoA) of the signal is important in propagation channel characterization. In our study, a conventional beamformer [6] is used. Although this method suffers from poor angular resolution, it does offer a linear and robust behavior. This method is also faster than high-resolution techniques because there is no value search and no iterative process. This beamformer structure is shown in Fig. 8.

Consider an array of N antennas whose far-field gains are denoted $a_1(\theta,\varphi),\cdots,a_N(\theta,\varphi)$. The received signals can be written as the vector $x = [x_1 \quad \cdots \quad x_N]^T$ where x_i represents the received signal by the i^{th} antenna. The weighting vector is $w(\theta,\varphi) = [w_1(\theta,\varphi),\cdots,w_N(\theta,\varphi)]$, where:

$$w_i(\theta,\varphi) = \frac{a_i^*(\theta,\varphi)}{\|a_i(\theta,\varphi)\|} \tag{4}$$

Then, the direction of arrival DoA is obtained by the linear combination of x and $w(\theta,\varphi)$.

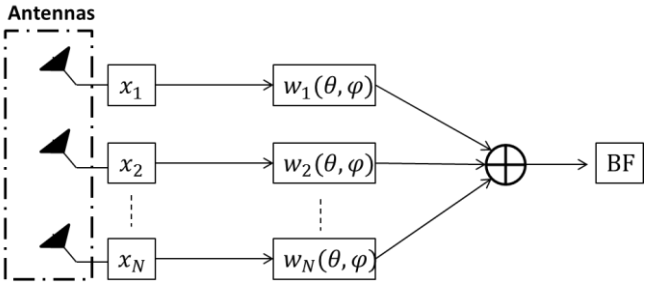

Fig. 8. Conventional beamformer

C. *Angular profile and Angular Spread*

During measurements, rays arrive at the receiver from different azimuth and elevation directions about the propagation scene. These distributions of multipath power are given as functions of azimuth angle φ and elevation angle θ. They are called azimuth and elevation power angular profile (PAP). The PAP at the receiver side was considered as the average of the PAPs of all N_{SIMO} single input multiple output (SIMO) links of the massive MIMO configuration (5). For each SIMO link, the PAP was computed by carrying out a directional analysis of the channel to find the DoA of rays.

$$\begin{cases} PAP(\theta) = \dfrac{1}{N_{SIMO}} \displaystyle\sum_{n=1}^{N_{SIMO}} |PAP_n(\theta)|^2 \\ PAP(\varphi) = \dfrac{1}{N_{SIMO}} \displaystyle\sum_{n=1}^{N_{SIMO}} |PAP_n(\varphi)|^2 \end{cases} \tag{5}$$

To characterize the angular dispersion of propagation channels, angular spread (AS) was evaluated. It characterizes the broadening of the signal over the incident angles due to the dispersive channel caused by the multipath propagation. The larger the angular spread, the higher is the space selecting fading. Also, a small angular spread means that the power is concentrated in one main path.. It should be noted that the definition of AS is non-trivial. Different definitions do indeed exist in the literature, such as Fleury [7] and 3GPP [8] methods. In this paper, the 3GPP method which is the most commonly applied one is used:

$$\sigma_\theta = \min_{\Delta} \sigma_\theta(\Delta) \tag{6}$$

$$\sigma_\theta(\Delta) = \sqrt{\frac{\sum_n(\theta_n + \Delta - \bar{\theta})^2 P_n}{\sum_n P_n}}, \qquad \bar{\theta} = \frac{\sum_n(\theta_n + \Delta)P_n}{\sum_n P_n}$$

where P_n is the power and θ_n the DoA of the nth rays, and Δ is a linear shift angle.

VI. Simulated and Measured Results

In this section, results are presented for two TX positions: TX3 in LoS at 17 m from RX antenna and Tx4 in NLoS at 27 m from RX antenna. For each TX position, PDPs, PAPs and DoA defined above are depicted. Angular and delay spreads are computed.

A. *LoS position: TX3*

Fig. 9 represents the measured and the simulated PDPs for LoS position TX3. It can be observed that most of the main rays have been found by Starlight simulation. However, the simulated PDP contains more energy than the measured one. This may be due to the differences between the database used by Starlight and the real environment. Indeed, Starlight models the ground and building as concrete blocks. This can also explain why some rays exist only in measurements but not in simulations like the one around 160 ns. Delay spreads were computed with a 25 dB threshold on the PDPs. The simulated delay spread ($\tau_{DS_s} = 32\ ns$) is larger than the measurements ($\tau_{DS_m} = 15\ ns$) because the simulated rays energy increases the multipath component.

Fig. 10 shows the measured and simulated DoA. As shown, it is possible to identify the main direction of arrival which is the same for both measurements and simulations. Furthermore, energy in other directions is observed. This is also seen in Fig. 11 and Fig. 12, where azimuth and elevation PAPs are represented.

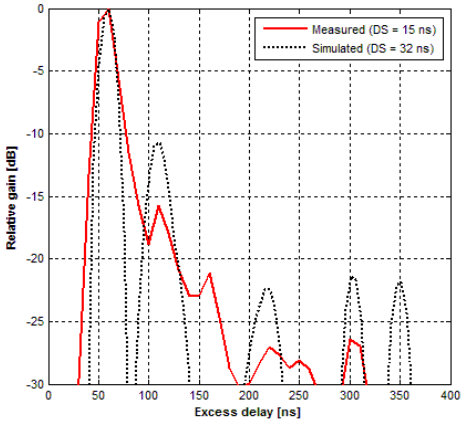

Fig. 9. Measured and simulated PDPs for LoS position TX3

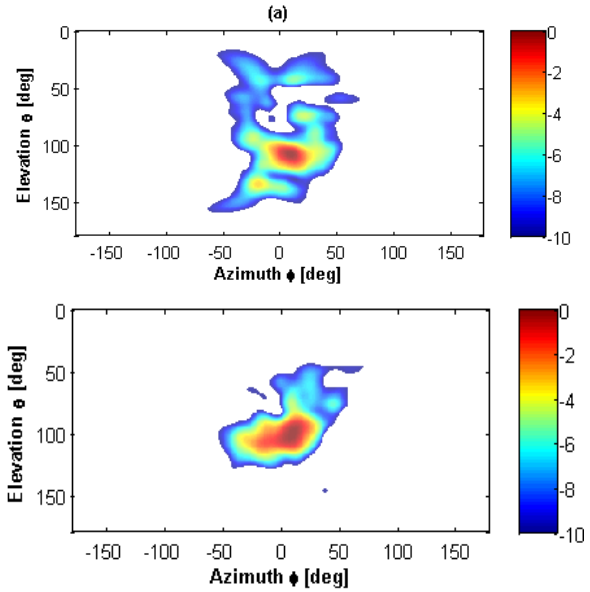

Fig. 10. Directions of arrival computed from: (a)- Measurements (b)- Simulations for LoS position TX3

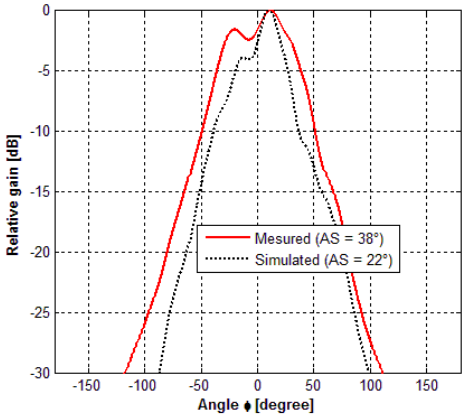

Fig. 11. Measured and simulated azimuth PAPs for LoS position TX3

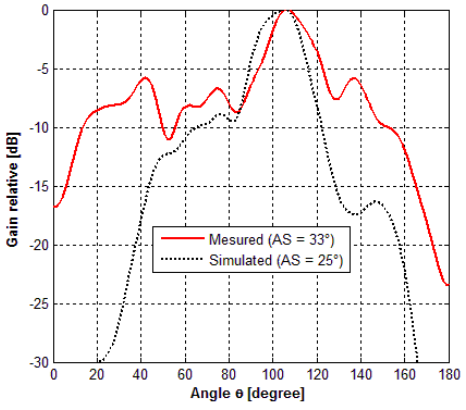

Fig. 12. Measured and simulated elevation PAPs for LoS position TX3

B. NLoS position: Tx4

The measured and the simulated PDPs for NLoS position Tx4 are represented in Fig. 13. Most of the simulated rays path are found in measurements but not with the same energy. Indeed, for measurements, we have two main paths with almost the same energy, but in simulations the first path who underwent one diffraction is weaker than others. The use of an inaccurate database may be the origin of this difference in ray energy. Delay spread have also been calculated with 25 dB of threshold: ($\tau_{DS_s} = 68\,ns$) for simulations, and ($\tau_{DS_m} = 40\,ns$). The delay spread in LoS is much smaller than in the NLOS for both measurements and simulations, because the multipath component are greater in NLoS. It should be noted that DS values in LoS and NLoS are lower than 100 ns.

The DoA computed for this position are shown in Fig. 14. Four directions of arrival are found for both measurements and simulations, with two main DoAs for measurement and one for simulations. Fig. 15 and Fig. 16 give PAPs for azimuth and elevation. In azimuth PAP main ray paths have been found, and elevation PAP shows a small offset between measurement and simulation. Actually, the observed discrepancies can be due to the uncertainties of the geographical and building database.

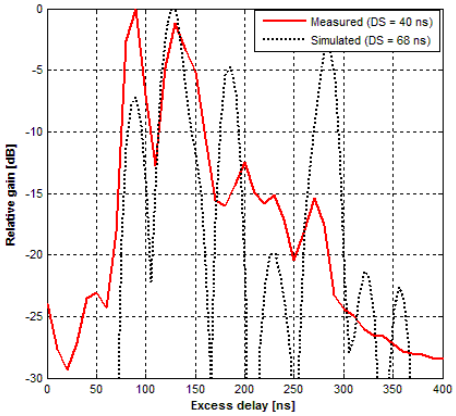

Fig. 13. Measured and simulated PDPs for NLoS position TX4

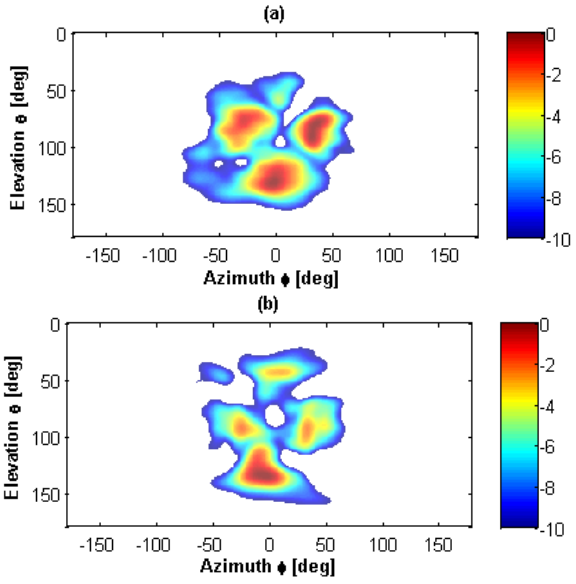

Fig. 14. Directions of arrival computed from: (a)- Measurements (b)- Simulations for NLoS position TX4

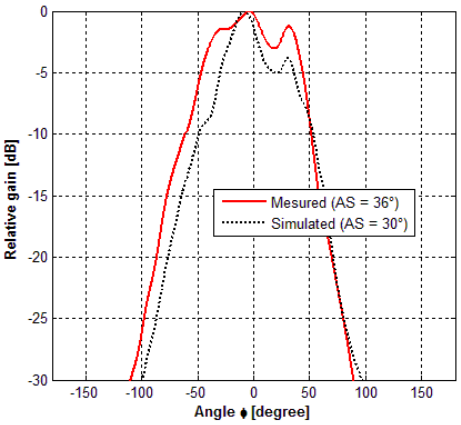

Fig. 15. Measured and simulated azimuth PAPs for LoS position Tx3

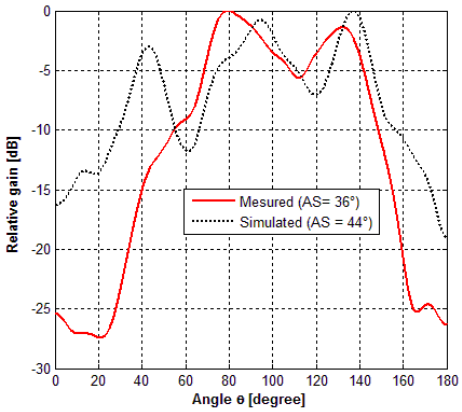

Fig. 16. Measured and simulated elevation PAPs for NLoS position Tx4

VII. Conclusion

In this paper, the measured and simulated massive MIMO propagation channel were studied. Measurements were carried out in a typical 5G context: at 3.7 GHz in an outdoor micro-cellular environment. Directions of arrival at the base station have been studied in order to determine the source of signals. Power delay and angular profiles as well as delay and angular spread values have been presented for two TX positions: one in LoS and the other in NLoS. Comparisons between measured and simulated PDPs revealed that most of the main rays have been found by Starlight. However, the simulated PDP contains more energy than the measured one. This may be due to the differences between the database used by Starlight and the actual measurement environment. Simulated delay spreads tend to be higher than measured ones, but their values are in agreement with literature [5][9]. Additionally, simulated angular spreads are lower than measured ones for LoS, and they are similar for NLoS.

Further work will study the capacity of massive MIMO propagation channels with real 5G antenna arrays to identify spectral efficiency gain according to radio configurations (micro, macro, frequency, geo database ...). A complete synthesis of the differences between measured and simulated channels depending on geo database accuracy should be done to increase Starlight model precision.

Acknowledgment

We thank P. Brun and C. Moroni for their help and skills for the campaign of measurements carried out in Belfort.

References

[1] https://spectrum.ieee.org/video/telecom/wireless/everything-you-need-to-know-about-5g

[2] P. Pajusco, F. Gallée, N. Malhouroux, R. Burghelea, “Massive antenna array for space-time channel sounding,” EuCAP 2017, Paris, March 19-24, 2017.

[3] P. Chambreuil, Y. Bénédic, “3-dimensional deterministic modeling of outdoor/indoor wave propagation,”IEEE VTC 2014-Fall, Vancouver, Canada.

[4] S. O. Kassap, “Principles of electronic materials and devices,” Third edition.

[5] S. Y. Seidel, T. S. Rappaport, and R. Singh, “Path loss and multipath delay statistics in four european cities for 900 MHz cellular and micro-cellular communications”, IEEE Transactions on Vehicular Technology, 1991.

[6] R. Müller et al., “Design of a circular antenna array for MIMO channel sounding application at 2.53 GHz,” The 8th European Conference on Antennas and Propagation (EuCAP 2014), The Hague, 2014, pp. 239-243.

[7] Fleury. B, “First- and second-order characterization of direction dispersion and space selectivity in the radio channel," Information theory, IEEE Transactions on 46(6), 2027-2044.

[8] 3GPP-3GPP2 SCM AHG, “SCM-135: Spatial channel model text description“, August 2003.

[9] N. Moraitis, A. Kanatas, G. Pantos, P. Constantinou, “Delay spread measurements and characterization in a special proapgation environment for pcs microcells,” The 13th IEEE International Symposium on Personal, Indoor and Mobile Communication (PIMRC 2002), Lisbon, Portugal.